

Chaotic Flower Pollination with Deep Learning Based COVID-19 Classification Model

T. Gopalakrishnan¹, Mohamed Yacin Sikkandar², Raed Abdullah Alharbi³, P. Selvaraj⁴, Zahraa H. Kareem⁵, Ahmed Alkhayyat^{6,*} and Ali Hashim Abbas⁷

¹Department of Information Technology, Manipal Institute of Technology Bengaluru, Manipal Academy of Higher Education, Manipal, India

²Department of Medical Equipment Technology, College of Applied Medical Sciences, Majmaah University, Al Majmaah, 11952, Saudi Arabia

³Public Health Department, College of Applied Medical Sciences, Majmaah University, Al Majmaah, 11952, Saudi Arabia

⁴Department of Computing Technologies, College of Engineering and Technology, Faculty of Engineering and Technology, SRM Institute of Science and Technology, Kattankulathur, 603203, Tamilnadu, India

⁵Medical Instrumentation Techniques Engineering Department, Al-Mustaqbal University College, Babylon, Iraq

⁶College of Technical Engineering, The Islamic University, Najaf, Iraq

⁷College of Information Technology, Imam Ja'afar Al-Sadiq University, Al-Muthanna, 66002, Iraq

*Corresponding Author: Ahmed Alkhayyat. Email: ahmedalkhayyat85@iunajaf.edu.iq

Received: 12 June 2022; Accepted: 12 October 2022

Abstract: The Coronavirus Disease (COVID-19) pandemic has exposed the vulnerabilities of medical services across the globe, especially in underdeveloped nations. In the aftermath of the COVID-19 outbreak, a strong demand exists for developing novel computer-assisted diagnostic tools to execute rapid and cost-effective screenings in locations where many screenings cannot be executed using conventional methods. Medical imaging has become a crucial component in the disease diagnosis process, whereas X-rays and Computed Tomography (CT) scan imaging are employed in a deep network to diagnose the diseases. In general, four steps are followed in image-based diagnostics and disease classification processes by making use of the neural networks, such as network training, feature extraction, model performance testing and optimal feature selection. The current research article devises a Chaotic Flower Pollination Algorithm with a Deep Learning-Driven Fusion (CFPA-DLDF) approach for detecting and classifying COVID-19. The presented CFPA-DLDF model is developed by integrating two DL models to recognize COVID-19 in medical images. Initially, the proposed CFPA-DLDF technique employs the Gabor Filtering (GF) approach to pre-process the input images. In addition, a weighted voting-based ensemble model is employed for feature extraction, in which both VGG-19 and the MixNet models are included. Finally, the CFPA with Recurrent Neural Network (RNN) model is utilized for classification, showing the work's novelty. A comparative analysis was conducted to demonstrate the enhanced performance of the proposed CFPA-DLDF model, and the results established the supremacy of the proposed CFPA-DLDF model over recent approaches.



This work is licensed under a Creative Commons Attribution 4.0 International License, which permits unrestricted use, distribution, and reproduction in any medium, provided the original work is properly cited.

Keywords: Deep learning; medical imaging; fusion model; chaotic models; ensemble model; COVID-19 detection

1 Introduction

Chest X-ray imaging is one of the promising techniques used in both diagnosis and the monitoring of several lung diseases such as pneumonia, tuberculosis, hernia infiltration and atelectasis [1,2]. COVID-19, a manifestation of lung infection and upper respiratory tract, was initially identified in Wuhan city, China, in late 2019. It majorly affects the airways and lungs of the infected individuals [3]. This deadly virus spread across the globe quickly and was announced as a pandemic by the World Health Organization (WHO). The number of cases and the resultant deaths have been increasing day-by-day since early 2020. Chest X-ray images are highly helpful in the prognosis of COVID-19 and detecting the impact caused by the disease upon the lung tissues. Subsequently, chest X-ray imaging has become a first-stage technique in detecting Coronavirus Disease (COVID-19) infection [4].

In automating processes like disease diagnosis and classification, the Computer-Aided Diagnosis (CAD) system offers important solutions to healthcare professionals and researchers in terms of detection and confirmation of the presence of coronavirus disease using novel classification techniques [5,6]. In this background, the CAD system has become an important domain of research. In COVID-19 disease diagnosis research, the CAD system uses Deep Learning (DL) or Machine Learning (ML) methods to evaluate all forms of a patient's data, including their clinical data images and forecast their disease conditions. This assessment method enhances the outcomes of the diagnostic procedures and assists the medical professionals in the decision-making process, which in turn enhances the prognosis as well [7]. Hence, the CAD mechanism is considered a powerful tool for radiotherapists to improve diagnostic approaches like chest radiographs, Computed Tomography (CT) scan and so on. Both DL and ML approaches were originally launched for the development of expert systems since these techniques play an important role in health care management, especially in the deployment of clinical decision support mechanisms [8]. These techniques not only support the classification of the diseases like muscle diseases, breast cancer, pneumonia and tuberculosis but are also helpful in the detection, diagnosis and classification of Coronavirus Disease (COVID-19) [9]. Further, DL and ML techniques are evolving technologies in the healthcare domain since these techniques are capable of producing highly-accurate prediction results, which is an important contribution to the healthcare automation process [10]. But, it is challenging to select the most appropriate DL or ML strategy since numerous strategies have been proposed and validated earlier, while most of the techniques render effectual results in the diagnosis of Coronavirus Disease (COVID-19).

Kumar et al. [11] presented a structure that collects small volumes of data from diverse sources (i.e., clinics) and trains the global DL method using a blockchain-related federated learning process. Blockchain (BC) technology validates the data, whereas the federated learning method trains the method worldwide. It helps in conserving the privacy of the organization. Initially, the authors presented a data normalization method to cover the heterogeneity of the data since it was collected from different hospitals using distinct forms of Computed Tomography (CT) scanners. Followed by the Capsule Network-related classification and segmentation were employed in the detection of Coronavirus Disease (COVID-19). Finally, a technique was devised to provide joint training to a global method with the help of BC technology and achieve federated learning during privacy preservation. In the study conducted earlier [12], the researchers proposed the MobileNet-V2 and VGG16 models using RMSprop and ADAM optimizers, respectively, for automatic detection of the Coronavirus Disease (COVID-19) from chest X-ray images and its differentiation from the rest of the pneumonia diseases.

Afterwards, the efficacy of the suggested method was improved by applying both Transfer Learning (TL) as well as data augmentation methods. These methods were utilized to address the overfitting issues.

Vaid et al. [13] devised a Deep Learning (DL) method to increase the accuracy of the reported cases and predict the disease using chest X-ray scan images. This method was developed based on the Convolutional Neural Networks (CNNs) method for detecting the disease and its categorization based on structural abnormalities. These structural abnormalities are the key entities that can reveal the hidden forms of Coronavirus Disease (COVID-19). So, a TL method was executed to recognize the presence of the disease in the chest anterior-posterior radiographs of the patients. In literature [14], a precise and effective DL CNN-related ensemble method was proposed using the DL technique. This study, 2,022 pneumonia cases were considered, whereas 5,863 normal chest X-ray images were collected from online resources and earlier publications. To improve the detection accuracy, both contrast enhancement and image normalization techniques were applied to produce high-quality images during the pre-processing stage itself. In the study conducted earlier [15], the authors mainly concentrated on the part of image processing or speech signals to detect the presence of Coronavirus Disease (COVID-19).

The current research article devises a Chaotic Flower Pollination Algorithm with a Deep Learning Driven Fusion (CFPA-DLDF) approach for detecting and classifying Coronavirus Disease (COVID-19). The presented CFPA-DLDF model is developed by integrating two DL models to identify the Coronavirus Disease (COVID-19) from the medical images. Initially, the proposed CFPA-DLDF technique employs the Gabor Filtering (GF) approach to pre-process the input images. In addition, a weighted voting-based ensemble model is employed for feature extraction in which both VGG-19 and MixNet models are included. Finally, the CFPA with Recurrent Neural Network (RNN) model is utilized for classification, which shows the novelty of the work. To demonstrate the enhanced performance of the proposed CFPA-DLDF model, a comparative study was conducted, and the results were discussed under different measures.

The rest of the paper is organized as follows. Section 2 discusses the proposed model, Section 3 details the performance validation of the model and Section 4 draws the conclusion for the study.

2 The Proposed Model

In the current study, a novel CFPA-DLDF technique has been developed for detection and the classification of Coronavirus Disease (COVID-19). The presented CFPA-DLDF model is developed by integrating two DL models to recognize the Coronavirus Disease (COVID-19) from the medical images. Initially, the proposed CFPA-DLDF technique exploits the GF approach to pre-process the input images. In addition, a weighted voting-based ensemble model is employed for feature extraction in which both VGG-19 and MixNet models are included. Finally, the CFPA model is utilized with the RNN model for classification, which shows the novelty of the work. Fig. 1 shows the block diagram of the CFPA-DLDF approach.

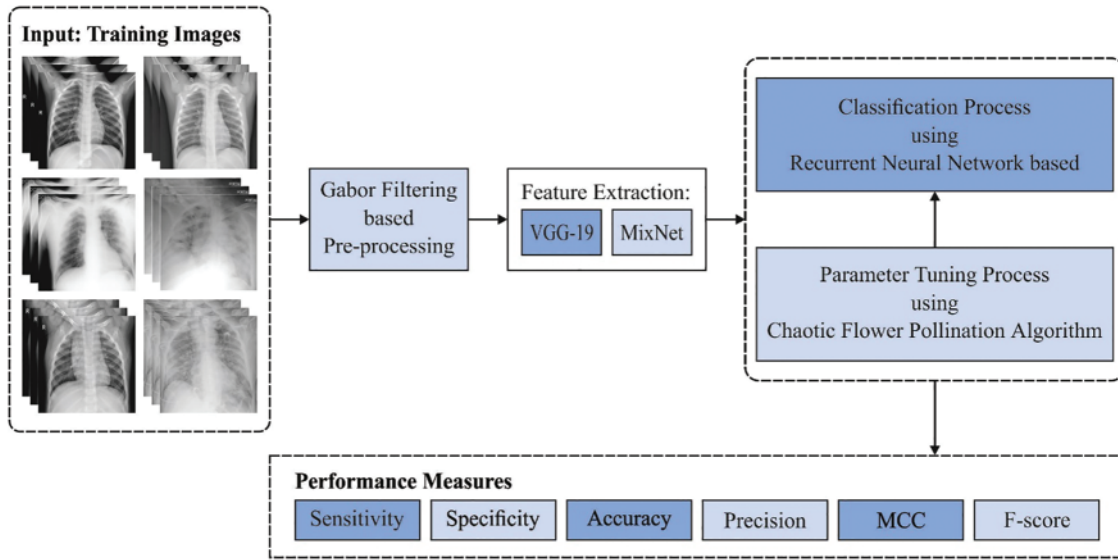


Figure 1: Block diagram of the CFPA-DLDF approach

2.1 Image Filtering

Initially, the CFPA-DLDF technique exploits the GF approach to pre-process the input image. GF, a bandpass filter, is a successful technique commonly applied in machine vision and image processing applications [16]. A two-dimensional GF is a complex sinusoidal grating that is modulated with the help of two-dimensional Gaussian envelope. The two dimensional coordinates are (a, b) , whereas the GF encompasses both real and imaginary components as given herewith.

$$G_{\delta, \theta, \psi, \sigma, \gamma}(a, b) = \exp\left(-\frac{a'^2 + \gamma^2 b'^2}{2\sigma^2}\right) \times \exp\left(j\left(2\pi\frac{a'}{\delta} + \psi\right)\right) \quad (1)$$

Here,

$$a' = a \cos \theta + b \sin \theta \quad (2)$$

$$b' = -a \sin \theta + b \cos \theta \quad (3)$$

At this point, θ indicates the orientation separation angle of the Gabor kernel, whereas δ describes the wavelength of the sinusoidal factor. Given that θ lies in the range of $[0^\circ, 180^\circ]$, ψ indicates the phase offset, σ denotes the standard derivation of the Gaussian envelope and $\psi = 0$ and $\psi = \pi/2$ correspond to imaginary and real parts of the GF. The parameter θ is determined to be 6, whereas the frequency bandwidth 'bw' is described with the help of Eq. (4).

$$\sigma = \frac{\delta}{\pi i} \sqrt{\frac{\ln 2}{2} \frac{2^{bw} + 1}{2^{bw} - 1}} \quad (4)$$

2.2 Fusion Based Feature Extraction

A weighted voting-based ensemble model is employed for feature extraction in which both VGG-19 and MixNet models are improved. In this weighted voting-based ensemble mechanism, a DL model is incorporated, and the maximal outcome is selected through weighted-voting mechanism. The voting

method is trained by each vector, after which a ten-fold cross validation accuracy is estimated with the help of a Fitness Function (FF). Assuming that n number of classes and D base classification models are fixed for voting, the prediction class c_k of the weighted voting for every instance k is determined as follows.

$$c_k = \arg \max_j \sum_{i=1}^D (\Delta_{ji} \times w_i), \quad (5)$$

In Eq. (5), Δ_{ji} represents the binary parameter. Once the i -th base classification model classifies k instance into j -th class, $\Delta_{ji} = 1$; then, $\Delta_{ji} = 0$. Here, w_i represents the weight of the i -th base classification mechanism. Then, the accuracy is determined as given below.

$$Acc = \frac{\sum_k \{1|c_k \text{ is the true class of instance } k\}}{\text{Size of test instances}} \times 100\%. \quad (6)$$

2.2.1 VGG-19 Model

CNN is the most commonly-used deep neural network technique in evaluating visual images. It is composed of neurons with learned biases and weights. Furthermore, it also contains hidden output and input layers. In a feedforward neural network, the middle layer is named as the hidden layer, whereas in the CNN method, the hidden layer is used for the implementation of the convolution layer. The CNN method has two primary models, as briefed herewith.

- Feature extraction or hidden layer: The network performs a sequence of pooling and convolution processes when a feature is identified.
- Classification: The full connection layer serves as a classification layer on top of the extracted feature by allocating a likelihood for the predicted objects.

VGG remains a novel component in CNN method after AlexNet [17]. VGG was originally conceived and developed in the name of ‘Visual Geometry Group’ at Oxford. The major involvement of VGG is to demonstrate that localisation or classification performance gets enhanced by increasing the depth of the CNN technique instead of utilizing it only in small receptive fields. VGG19 is a CNN method and has a total of 19 layers as briefed herewith.

- It has a fixed input size of $224 * 224$. For an RGB image, the input can be transformed to $224 * 224 * 3$. Here, two 224 values denote the height and the weight, respectively, whereas ‘3’ corresponds to the RGB channel.
- A kernel of $3 * 3$ using a stride size of 1 pixel.
- A max pooling of $2 * 2$ -pixel window using a stride of 2.
- A Rectified Linear Unit (ReLU) for nonlinearity operation (the preceding modes utilize sigmoid or \tanh).
- It has a tree FC layer in which the two initial layers have a size of 4096, whereas the final layer has 1,000 channels that are class-counted in ImageNet datasets.
- The layer comprises a *Softmax* function.

2.2.2 MixNet Model

CNN model, developed on the basis of traditional convolution operation, is challenging to apply in real-time scenarios. This is attributed to the presence of numerous parameters in it with complex calculations. A sequence of lightweight convolution operators is presented to increase the accuracy of the model. Depthwise separable convolutional layer is the commonly-applied lightweight convolution operator [18]. It can be divided into pointwise- and depthwise-convolutions. Initially, it convolutes a

single channel at a time using a convolution kernel sized at 3. Next, it makes use of a feature map with 1×1 convolution kernel. Given that $N D_k \times D_k$ corresponds to a feature view, 1 convolutional sliding step is applied in the convolution of the feature map with $D_F \times D_F \times M$ dimensions. The output feature map with $D_F \times D_F \times N$ dimensions is involved as given below.

$$D_k \times D_k \times M \times N \quad (7)$$

The parameters, included in a depth-wise separable convolution operation, are shown below.

$$D_k \times D_k \times M + 1 \times 1 \times M \times N \quad (8)$$

The computation, included in the traditional convolution operation, is given herewith.

$$D_k \times D_k \times M \times N \times D_F \times D_F \quad (9)$$

The computation, included in a depth-wise separable convolution operation, is described herewith.

$$D_k \times D_k \times M \times D_F \times D_F \times M \times N \times D_F \times D_F \quad (10)$$

The ratio of the two operations is given below.

$$\frac{D_k \times D_k \times M \times D_F \times D_F \times M \times N \times D_F \times D_F}{D_k \times D_k \times M \times N \times D_F \times D_F} \quad (11)$$

A depth-wise separable convolution employs a comparable size of 3×3 convolution kernels in the computation model; but, a network with large convolution kernels such as 5×5 or 7×7 confirms that a large convolution kernel enhances both accuracy as well as efficiency of the module. But the experiment demonstrates that it is rare to achieve a large and a better convolution kernel; at the same time, a large convolution kernel can reduce the accuracy of the model. Now, the MDConv splits the input channel sized M into C groups. Then, it convolves each and every group with kernels of dissimilar sizes. The depth-wise separable convolutions split the M -sized input channel into M groups after which the convolution calculation is performed for every group with a comparable kernel size.

2.3 RNN-Based Image Classification

In this study, the RNN technique is utilized for the purpose of classification [19]. A basic RNN structure, as given in Fig. 2, has a hidden layer, an output layer and an input layer. Assume a sequential sample of length, $x = [x_1, x_2, x_3, \dots, x_{T-1}, x_T]$, RNN reads x in the order of x_1 to x_T , computes the hidden state h_t and output 0_t by iterating the subsequent equations from $t = 1$ to T

$$h_t = f(W_{xh} \cdot x_t + W_{hh} \cdot h_{t-1}), t = 1 \dots T \quad (12)$$

$$0_t = f(W_{hx} \cdot h_t), t = 1 \dots T \quad (13)$$

Here, $W_{xh} \in \mathbb{R}^{m \times d}$, $W_{hh} \in \mathbb{R}^{m \times m}$ and $W_{hx} \in \mathbb{R}^{m \times n}$ indicate the weights of the input-hidden, hidden-hidden and hidden-output correspondingly. Further, d , m & n denote the sizes of the input, hidden, and output layers respectively. Likewise, $f(\cdot)$ denotes the activation operation that functions on every component. In general, the last output 0_T is utilized as a Softmax classifier feature for the prediction of the label, since it contains the data for the entire sequential data, x . Owing to the outstanding modelling of the sequential data, the RNN method attains a state-of-the-art performance on the classification procedures.

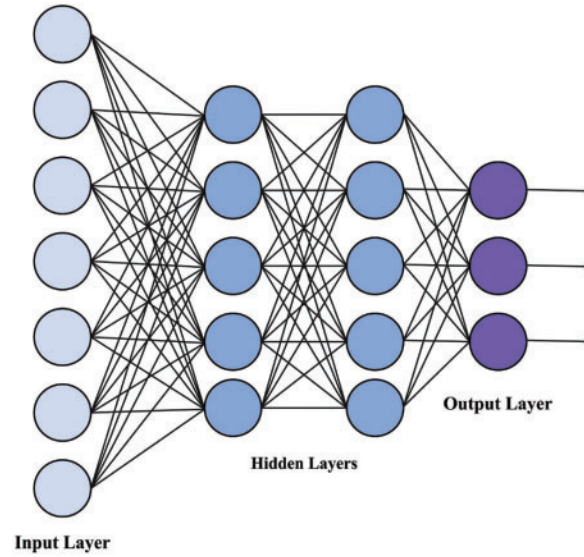


Figure 2: Framework of the RNN model

2.4 CFPA Based Hyperparameter Tuning

The CFPA model is used to fine-tune the hyperparameters [20–24] involved in the RNN model. It is a modified metaheuristic approach that was improved by adapting a major concept from FPA. The FPA model was initially developed as a simulation of natural processes [25]. The CFPA model has two major evolutionary phases namely, local and global pollination. Unlike the former approach, i.e., the novel FPA which uses the data of the finest individual from the existing generation, the presented algorithm considers the information of the entire population. The global pollination is mathematically expressed as given herewith.

$$S_i^{t+1} = S_i^t + \alpha(t) L_1(\lambda) (S_i^t - g^*) + \beta(t) L_2(\lambda) C_i^t \tag{14}$$

In Eq. (14), the *i*-th pollen or the solution vector S_i at *t*-th generation is represented by S_i^t , while the vector representation for data of the population, with respect to *i*-th individual at *t*-th generation, is denoted by C_i^t . The constants, associated with the problem scale at *t*-th generation, are indicated by $\alpha(t)$ and $\beta(t)$. The existing optimal individuals found amongst the population in the present generation are represented by g^* . In this technique, the Levy flight is applied by the CFPA model. However, the expression is dissimilar to the one that is utilized in the Enhanced Cuckoo Search algorithm. To be specific, the variable L_1 refers to the power of the pollination and is derived from Levy distribution.

$$L_1(\lambda) \sim \frac{\lambda \Gamma(\lambda) \sin(\pi\lambda/2)}{\pi} \frac{1}{t^{1+\lambda}} \tag{15}$$

$$L_2(\lambda) = t^{-\lambda} (\lambda \in [1, 3]) \tag{16}$$

In this equation, the standard gamma function is represented by $\Gamma(\lambda)$ and the distribution is effective for a large step, $t > 0$. The current iteration is denoted by *t* and the scaling factor to control the step size is denoted by λ . Like ICS, the CFPA method too employs a similar functionalization for α and β .

$$\alpha(t) = \alpha_{\max} e^{\frac{t}{T} \ln(\frac{\alpha_{\min}}{\alpha_{\max}})} \tag{17}$$

$$\beta(t) = \beta_{\max} e^{\frac{t}{T} \ln\left(\frac{\beta_{\min}}{\beta_{\max}}\right)} \quad (18)$$

$$p(t) = p_{\max} - \frac{t}{T} (p_{\max} - p_{\min}) \quad (19)$$

In the equations given above, p_{\max} and p_{\min} denote the upper and the lower bounds of the global pollination possibility values. Further, $p(t)$ corresponds to the possibility of the global pollination at t -th generation. α_{\max} and α_{\min} denote the maximum and minimum values of α . β_{\max} and β_{\min} indicate the maximum and minimum values of β . T refers to the maximal number of generations. The index of the existing generation is denoted by t .

At the time of global pollination, the CFPA approach applies the dataset of the existing population. Here, C_i^t denotes the vector representation of the population data with regards to i -th individual at t -th generation. To be specific, C_i^t can be evaluated using the following equation.

$$C_i^t = \sum_k Q_{ik}^t (S_k^t - S_i^t) \quad (20)$$

In Eq. (20), $Q_{ik}(t)$ represents the contribution of the k -th individual to C_i^t and is evaluated as follows.

$$Q_{ik} = \frac{\sum_{ik} \frac{\text{maxfitness}(S)}{\text{fitness}(S_k)}}{\sum_{j=1}^n \sum_{ik} \frac{\text{maxfitness}(S)}{\text{fitness}(S_k)}} \quad (21)$$

$$E_{ik} = \begin{cases} 1 & \text{when fitness}(S_k) < \text{fitness}(S_i) \\ 0 & \text{elsewhere} \end{cases} \quad (22)$$

The aim of this amendment is to increase the global search process that is crucial for localizing the situation of the optimum solution. It minimizes the possibility of the ‘bad’ outcomes that are produced by randomly-initialized poor solutions and broadens the search scale of the proposed algorithm. Having been exaggerated by flower constancy and local pollination, the updated individual process is given below.

$$S_i^{t+1} = S_i^t + \varepsilon (S_j^t - S_k^t) \quad (23)$$

In Eq. (23) S_j^t and S_k^t denote the pollens from dissimilar flowers of the identical species. ε is derived from standard distribution that lies between 0 and 1. At last, a switching possibility is promised between local and the global pollinations.

3 Results and Discussion

The presented model was experimentally validated using a dataset with 6,448 samples under two classes namely, COVID and healthy and the dataset details are shown in Table 1.

Fig. 3 portrays the confusion matrices generated by the proposed CFPA-DLDF model with distinct training (TR) and testing (TS) datasets. On 70% of TR data, the proposed CFPA-DLDF model categorized 2,203 samples under COVID class and 2,255 samples under healthy class. Also, on 30% of TS data, the CFPA-DLDF approach classified 955 samples under COVID class and 952 samples under healthy class. In addition, on 20% of TS data, the presented CFPA-DLDF system recognized 651 samples under COVID class and 628 samples under healthy class respectively.

Table 1: Dataset details

Class	No. of images
COVID	3224
Healthy	3224
Total number of images	6448

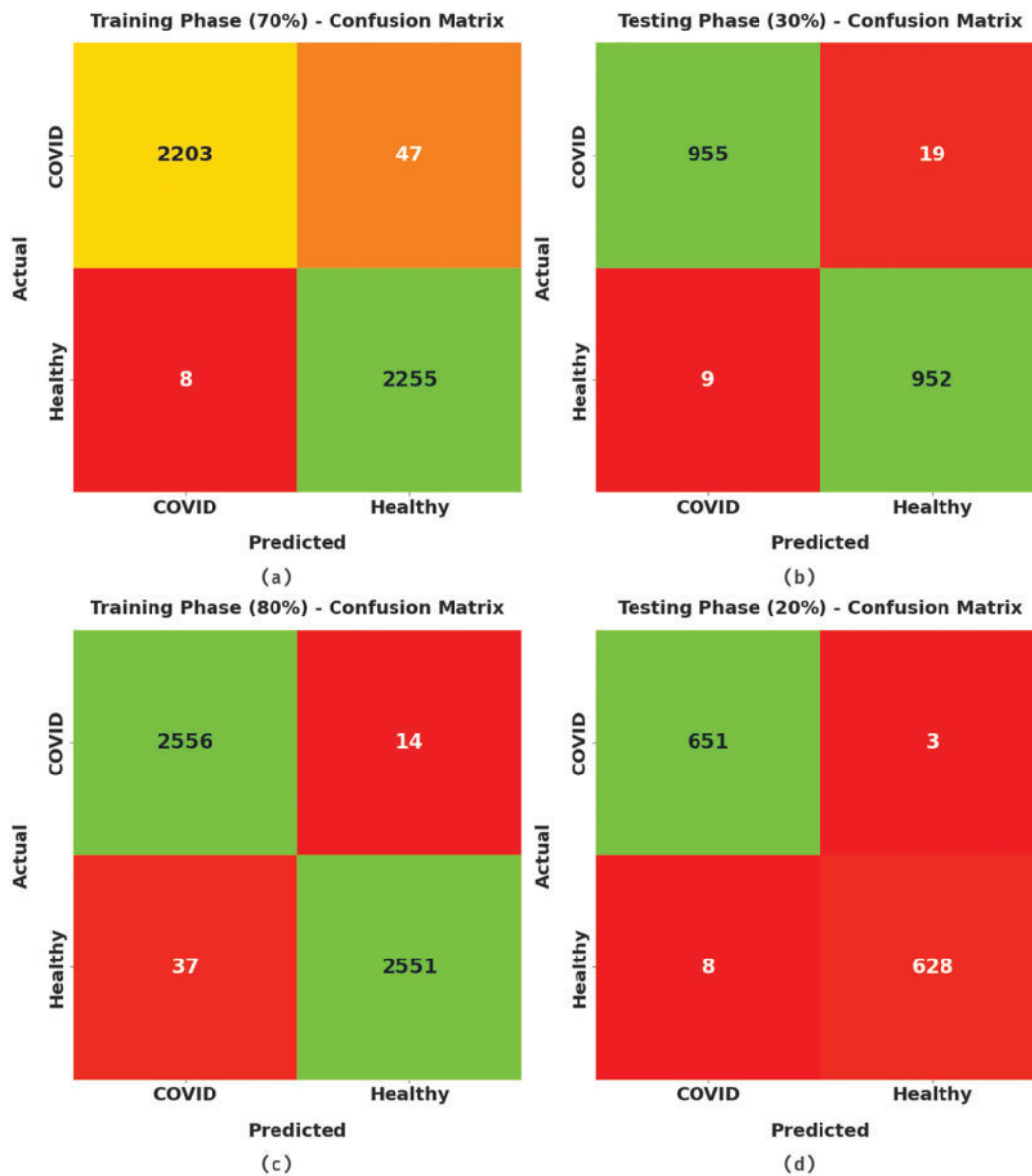


Figure 3: Confusion matrices of CFPA-DLDF approach (a) 70% of TR data, (b) 30% of TS data, (c) 80% of TR data, and (d) 20% of TS data

Table 2 and Fig. 4 provide a detailed overview on the classification outcomes achieved by the CFPA-DLDF model using 70% TR data and 30% TS data. The results imply that the proposed CFPA-DLDF model achieved improved outcomes. For instance, with 70% of TR data, the proposed CFPA-DLDF model reached an average $accu_y$ of 98.78%, $prec_n$ of 98.80%, $sens_y$ of 98.78%, $spec_y$ of 98.78% and an F_{score} of 98.78%. Also, with 30% of TR data, the presented CFPA-DLDF approach attained an average $accu_y$ of 98.55%, $prec_n$ of 98.55%, $sens_y$ of 98.56%, $spec_y$ of 98.56% and an F_{score} of 98.55%.

Table 2: Results of the analysis of the CFPA-DLDF approach under different measures using 70% TR and 30% TS datasets

Labels	Accuracy	Precision	Sensitivity	Specificity	F-score
Training phase (70%)					
COVID	98.78	99.64	97.91	99.65	98.77
Healthy	98.78	97.96	99.65	97.91	98.80
Average	98.78	98.80	98.78	98.78	98.78
Testing phase (30%)					
COVID	98.55	99.07	98.05	99.06	98.56
Healthy	98.55	98.04	99.06	98.05	98.55
Average	98.55	98.55	98.56	98.56	98.55

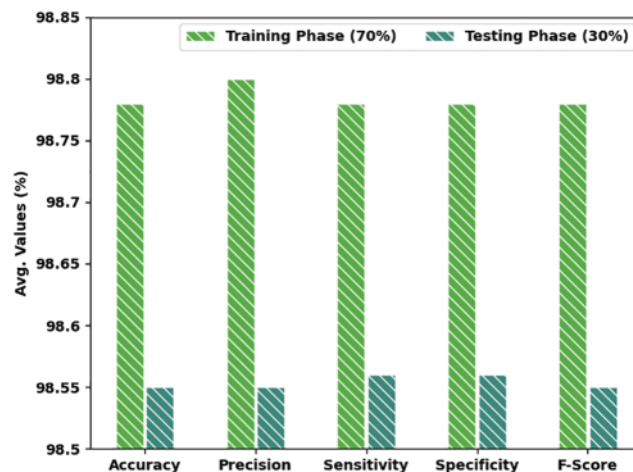


Figure 4: Average analysis results of the CFPA-DLDF approach under 70% TR and 30% TS datasets

Table 3 and Fig. 5 present a brief overview on the classification outcomes accomplished by the proposed CFPA-DLDF method on 80% TR data and 20% TS datasets. The results infer that the presented CFPA-DLDF technique achieved enhanced results. For example, with 80% TR data, the CFPA-DLDF approach achieved an average $accu_y$ of 99.01%, $prec_n$ of 99.01%, $sens_y$ of 99.01%, $spec_y$ of 99.01 and an F_{score} of 99.01%. Additionally, with 20% of TR data, the proposed CFPA-DLDF methodology obtained an average $accu_y$ of 99.15%, $prec_n$ of 99.16%, $sens_y$ of 99.14%, $spec_y$ of 99.14% and an F_{score} of 99.15%.

Table 3: Results of the analysis of the CFPA-DLDF approach under different measures using 80% TR and 20% TS datasets

Labels	Accuracy	Precision	Sensitivity	Specificity	F-score
Training phase (80%)					
COVID	99.01	98.57	99.46	98.57	99.01
Healthy	99.01	99.45	98.57	99.46	99.01
Average	99.01	99.01	99.01	99.01	99.01
Testing phase (20%)					
COVID	99.15	98.79	99.54	98.74	99.16
Healthy	99.15	99.52	98.74	99.54	99.13
Average	99.15	99.16	99.14	99.14	99.15

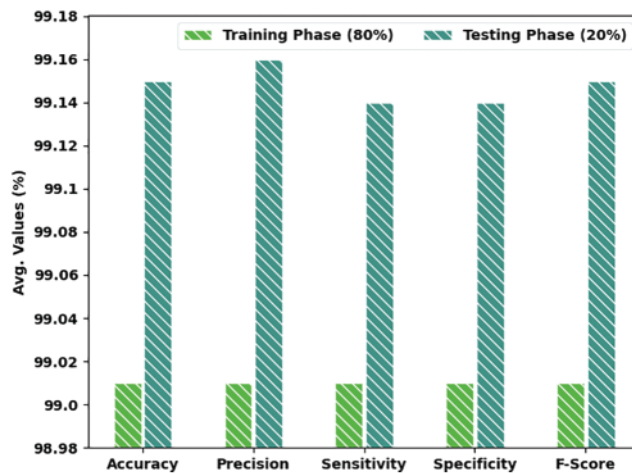


Figure 5: Average analysis results of the CFPA-DLDF approach under 80% TR and 20% TS datasets

Both Training Accuracy (TA) and Validation Accuracy (VA) values, acquired by the proposed CFPA-DLDF approach on test dataset, are illustrated in Fig. 6. The experimental outcomes infer that the proposed CFPA-DLDF method reached the maximum TA and VA values whereas VA values were higher than the TA values.

Both Training Loss (TL) and Validation Loss (VL) values, attained by the proposed CFPA-DLDF method on test dataset, are showcased in Fig. 7. The experimental outcomes infer that the proposed CFPA-DLDF algorithm achieved the minimal TL and VL values whereas VL values were lower than the TL values.

A clear precision-recall analysis was conducted upon the CFPA-DLDF technique using the test dataset and the results are displayed in Fig. 8. The figure infers that the proposed CFPA-DLDF algorithm achieved enhanced precision-recall values under all the classes.

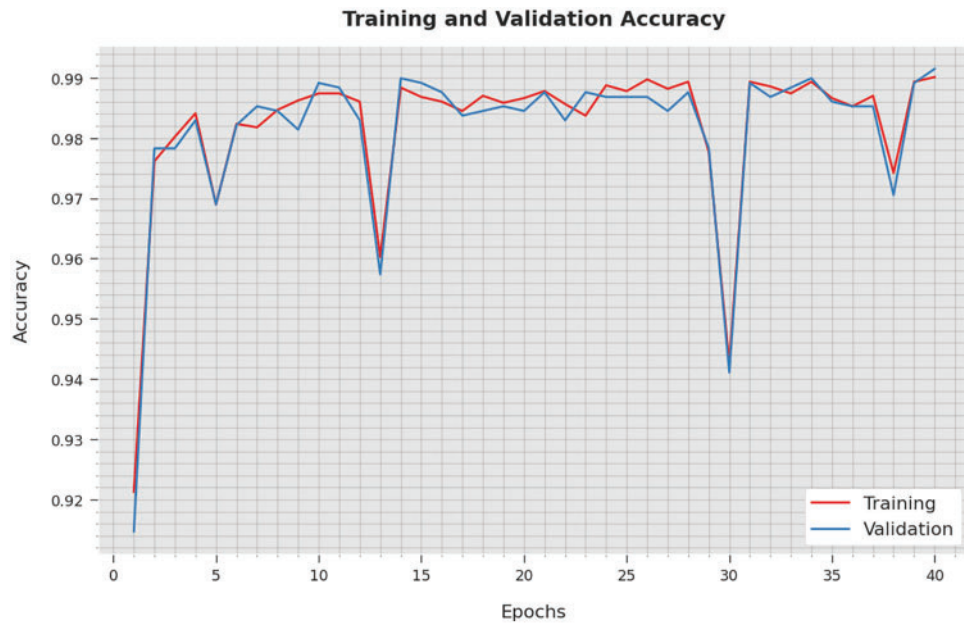


Figure 6: TA and VA analyses results of the CFPA-DLDF method

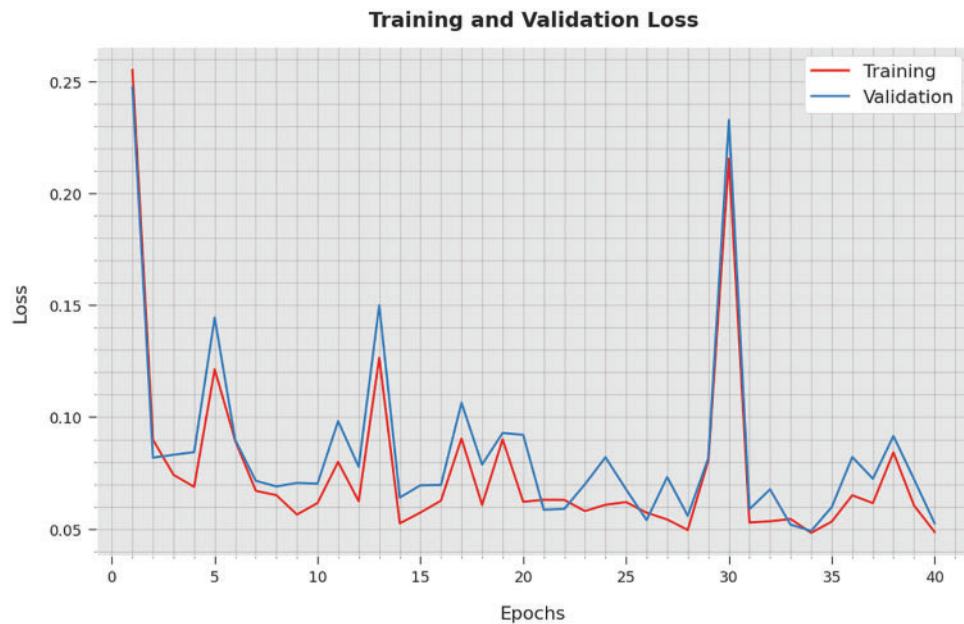


Figure 7: TL and VL analyses results of the CFPA-DLDF method

A brief Receiver Operating Characteristic (ROC) scrutiny analysis was conducted upon the CFPA-DLDF methodology using the test dataset and the results are illustrated in Fig. 9. The results indicate that the proposed CFPA-DLDF method exhibited its ability in categorized the dataset under distinct classes.

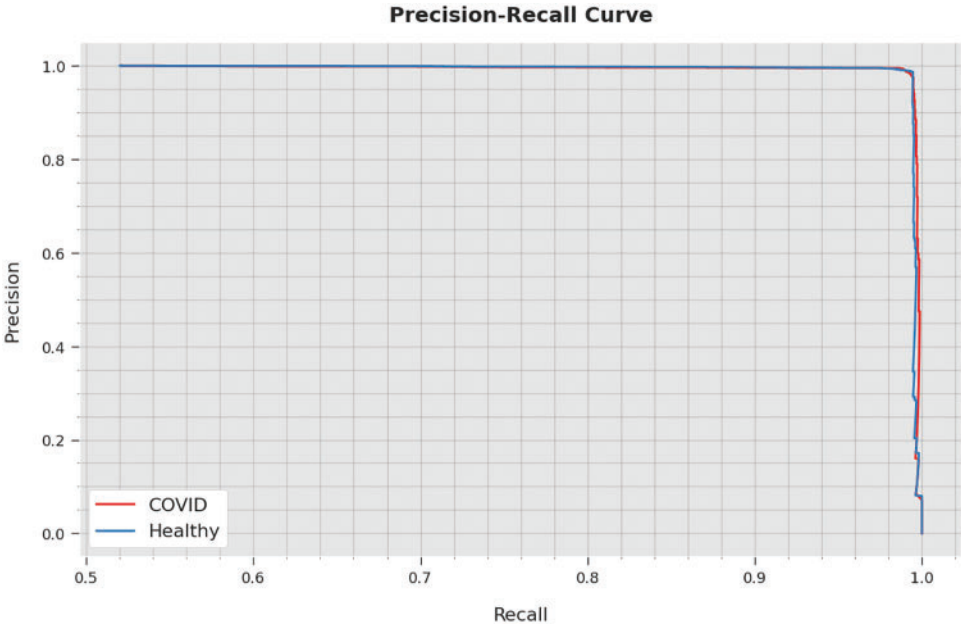


Figure 8: Precision-recall curve analysis results of the CFPA-DLDF method

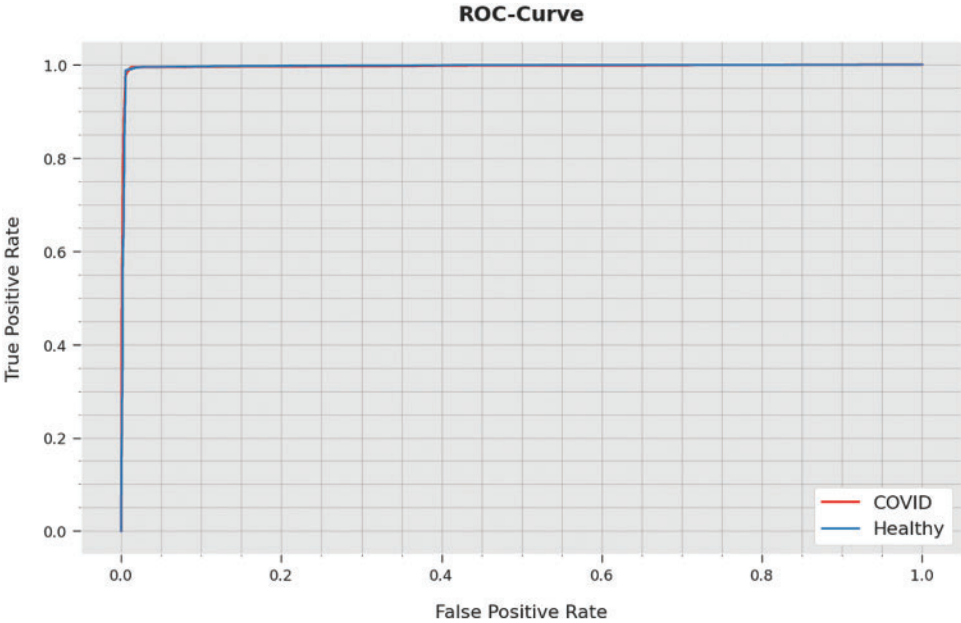


Figure 9: ROC curve analysis results of the CFPA-DLDF method

Table 4 demonstrates the overall comparative study results accomplished by the proposed CFPA-DLDF model and other recent models.

Table 4: Comparative analysis results of the CFPA-DLDF approach and other recent methodologies

Methods	Accuracy	Precision	Sensitivity	Specificity
CFPA-DLDF	99.15	99.16	99.14	99.14
InceptionResNet-v2	96.66	96.70	94.65	97.23
Inception-v3	95.23	97.79	94.67	95.84
ResNet101	95.49	94.18	96.61	94.09
VGG-19	97.13	95.07	96.20	96.40
COVID-Net	94.66	95.40	94.07	97.16
DarkCovidNet	94.48	96.46	94.38	94.54

Fig. 10 demonstrates the comparison study results achieved by the proposed CFPA-DLDF model and other existing models in terms of $accu_y$. The figure implies that both COVID-Net and the DarkCovidNet models achieved the least $accu_y$ values such as 94.66% and 94.48% respectively. Likewise, the other models such as Inception-v3, ResNet101 and InceptionResNet-v2 models accomplished moderately increased $accu_y$ values such as 95.23%, 95.49% and 96.66%. Though the VGG-19 gained a reasonable $accu_y$ of 97.13%, the proposed CFPA-DLDF model accomplished the highest $accu_y$ of 99.15%.

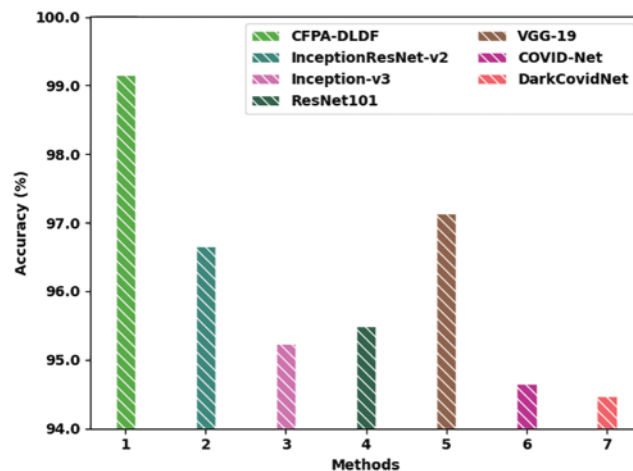
**Figure 10:** $Accu_y$ analysis results of the CFPA-DLDF approach and other recent methodologies

Fig. 11 signifies the comparative analysis outcomes accomplished by the proposed CFPA-DLDF method and other existing models in terms of $prec_n$. The figure implies that both COVID-Net and DarkCovidNet models produced the least $prec_n$ values such as 95.40% and 96.46% correspondingly. Also, the other models such as Inception-v3, ResNet101 and InceptionResNet-v2 techniques established moderately increased $prec_n$ values such as 97.79%, 94.18% and 96.70% respectively. Though the VGG-19 model reached a reasonable $prec_n$ of 95.07%, the proposed CFPA-DLDF method accomplished the highest $prec_n$ of 99.16%.

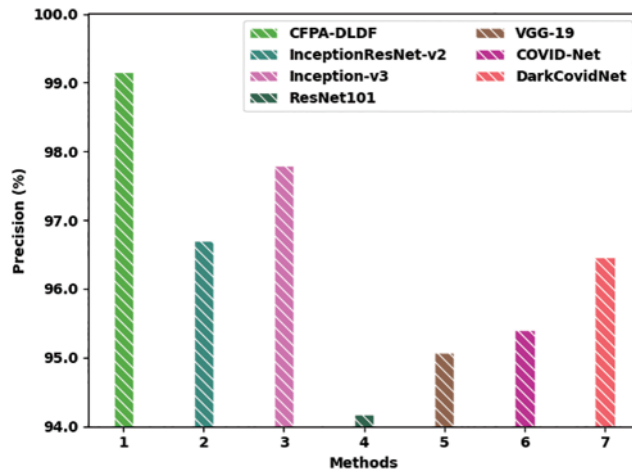


Figure 11: $Prec_n$ analysis results of the CFPA-DLDF approach and other recent methodologies

Fig. 12 illustrates the detailed inspection outcomes of the proposed CFPA-DLDF technique and other existing models in terms of $sens_y$. The figure denotes that both COVID-Net and DarkCovidNet algorithms produced the least $sens_y$ values such as 94.07% and 94.38% correspondingly. Moreover, the other models such as Inception-v3, ResNet101 and InceptionResNet-v2 models accomplished moderately increased $sens_y$ values such as 94.67%, 96.61% and 94.65% correspondingly. Though the VGG-19 model acquired a reasonable $sens_y$ of 96.20%, the proposed CFPA-DLDF method accomplished the highest $sens_y$ of 99.14%.

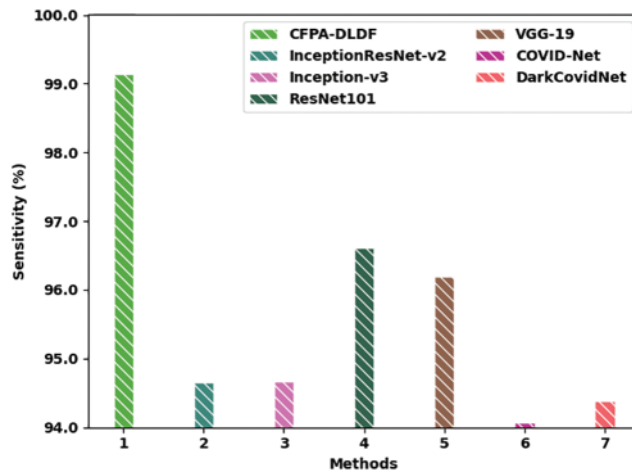


Figure 12: $Sens_y$ analysis results of the CFPA-DLDF approach and other recent methodologies

Fig. 13 shows the results of the comparison analysis conducted between the proposed CFPA-DLDF method and other existing models in terms of $spec_y$. The figure displays that both COVID-Net and DarkCovidNet techniques produced the least $spec_y$ values such as 97.16% and 94.54% correspondingly. Furthermore, the other models such as Inception-v3, ResNet101 and InceptionResNet-v2 established moderately increased $spec_y$ values such as 95.84%, 94.09% and 97.23% respectively. Though the VGG-19 model achieved a reasonable $spec_y$ of 96.40%, the proposed CFPA-DLDF algorithm achieved a maximum $spec_y$ of 99.14%.

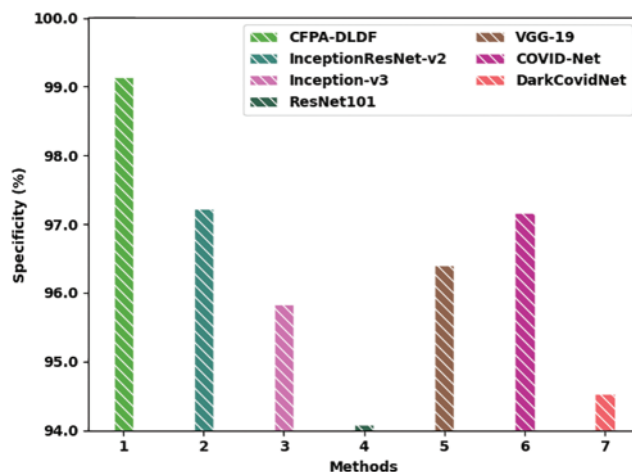


Figure 13: *Spec_y* analysis results of the CFPA-DLDF approach and other recent methodologies

4 Conclusion

In this work, a novel CFPA-DLDF technique has been developed for detection and the classification of the Coronavirus Disease (COVID-19). The presented CFPA-DLDF model is developed by integrating two DL models to recognize the Coronavirus Disease (COVID-19) from the medical images. Initially, the proposed CFPA-DLDF technique exploits the GF approach to pre-process the input image. In addition, a weighted voting-based ensemble model is deployed as a feature extractor in which both VGG-19 and MixNet models are included. Finally, the CFPA is utilized with RNN model for the purpose of classification, which shows the novelty of the work. To demonstrate the enhanced performance of the proposed CFPA-DLDF model, a comparative study was conducted and the results established the supremacy of the proposed CFPA-DLDF model over recent approaches. In the future, the performance of the CFPA-DLDF model can be improved with the help of contrast improvement approaches.

Funding Statement: The authors received no specific funding for this study.

Conflicts of Interest: The authors declare that they have no conflicts of interest to report regarding the present study.

References

- [1] G. Jain, D. Mittal, D. Thakur and M. K. Mittal, "A deep learning approach to detect COVID-19 coronavirus with X-ray images," *Biocybernetics and Biomedical Engineering*, vol. 40, no. 4, pp. 1391–1405, 2020.
- [2] A. Rehman, T. Saba, U. Tariq and N. Ayesha, "Deep learning-based COVID-19 detection using CT and x-ray images: Current analytics and comparisons," *IT Professional*, vol. 23, no. 3, pp. 63–68, 2021.
- [3] D. Brinati, A. Campagner, D. Ferrari, M. Locatelli, G. Banfi *et al.*, "Detection of COVID-19 infection from routine blood exams with machine learning: A feasibility study," *Journal of Medical Systems*, vol. 44, no. 8, pp. 135, 2020.
- [4] A. Rehman, M. A. Iqbal, H. Xing and I. Ahmed, "COVID-19 detection empowered with machine learning and deep learning techniques: A systematic review," *Applied Sciences*, vol. 11, no. 8, pp. 3414, 2021.

- [5] M. Roberts, D. Driggs, M. Thorpe, J. Gilbey, M. Yeung *et al.*, “Common pitfalls and recommendations for using machine learning to detect and prognosticate for COVID-19 using chest radiographs and CT scans,” *Nature Machine Intelligence*, vol. 3, no. 3, pp. 199–217, 2021.
- [6] F. Saiz and I. Barandiaran, “COVID-19 detection in chest x-ray images using a deep learning approach,” *International Journal of Interactive Multimedia and Artificial Intelligence*, vol. 6, no. 2, pp. 1–4, 2020.
- [7] M. A. Salam, S. Taha and M. Ramadan, “COVID-19 detection using federated machine learning,” *PLoS One*, vol. 16, no. 6, pp. e0252573, 2021.
- [8] S. Akter, F. M. J. M. Shamrat, S. Chakraborty, A. Karim and S. Azam, “COVID-19 detection using deep learning algorithm on chest x-ray images,” *Biology*, vol. 10, no. 11, pp. 1174, 2021.
- [9] T. Zebin and S. Rezvy, “COVID-19 detection and disease progression visualization: Deep learning on chest X-rays for classification and coarse localization,” *Applied Intelligence*, vol. 51, no. 2, pp. 1010–1021, 2021.
- [10] J. I. Z. Chen, “Design of accurate classification of COVID-19 disease in x-ray images using deep learning approach,” *Journal of ISMAC*, vol. 2, no. 2, pp. 132–148, 2021.
- [11] R. Kumar, A. A. Khan, J. Kumar, N. A. Golilarz, S. Zhang *et al.*, “Blockchain-federated-learning and deep learning models for COVID-19 detection using CT imaging,” *IEEE Sensors Journal*, vol. 21, no. 14, pp. 16301–16314, 2021.
- [12] H. Swapnarekha, H. S. Behera, D. Roy, S. Das and J. Nayak, “Competitive deep learning methods for COVID-19 detection using x-ray images,” *Journal of the Institution of Engineers (India): Series B*, vol. 102, no. 6, pp. 1177–1190, 2021.
- [13] S. Vaid, R. Kalantar and M. Bhandari, “Deep learning COVID-19 detection bias: Accuracy through artificial intelligence,” *International Orthopaedics (SICOT)*, vol. 44, no. 8, pp. 1539–1542, 2020.
- [14] P. Bhardwaj and A. Kaur, “A novel and efficient deep learning approach for COVID -19 detection using X-ray imaging modality,” *International Journal of Imaging Systems and Technology*, vol. 31, no. 4, pp. 1775–1791, 2021.
- [15] A. B. Nassif, I. Shahin, M. Bader, A. Hassan and N. Werghi, “COVID-19 detection systems using deep-learning algorithms based on speech and image data,” *Mathematics*, vol. 10, no. 4, pp. 564, 2022.
- [16] P. Malaca, L. F. Rocha, D. Gomes, J. Silva and G. Veiga, “Online inspection system based on machine learning techniques: Real case study of fabric textures classification for the automotive industry,” *Journal of Intelligent Manufacturing*, vol. 30, no. 1, pp. 351–361, 2019.
- [17] A. R. Khan, S. Khan, M. Harouni, R. Abbasi, S. Iqbal *et al.*, “Brain tumor segmentation using K-means clustering and deep learning with synthetic data augmentation for classification,” *Microscopy Research and Technique*, vol. 84, no. 7, pp. 1389–1399, 2021.
- [18] E. Amrutha, S. Arivazhagan and W. S. L. Jebarani, “MixNet: A robust mixture of convolutional neural networks as feature extractors to detect stego images created by content-adaptive steganography,” *Neural Processing Letters*, vol. 54, no. 2, pp. 853–870, 2022.
- [19] M. A. Khan, “HCRNNIDS: Hybrid convolutional recurrent neural network-based network intrusion detection system,” *Processes*, vol. 9, no. 5, pp. 834, 2021.
- [20] K. Shankar, E. Perumal, M. Elhoseny, F. Taher, B. B. Gupta *et al.*, “Synergic deep learning for smart health diagnosis of COVID-19 for connected living and smart cities,” *ACM Transactions on Internet Technology*, vol. 22, no. 3, pp. 16: 1–14, 2022.
- [21] K. Shankar, E. Perumal, V. G. Díaz, P. Tiwari, D. Gupta *et al.*, “An optimal cascaded recurrent neural network for intelligent COVID-19 detection using chest X-ray images,” *Applied Soft Computing*, vol. 113, Part A, pp. 1–13, 2021.
- [22] M. Y. Sikkandar, B. A. Alrasheadi, N. B. Prakash, G. R. Hemalakshmi, A. Mohanarathinam *et al.*, “Deep learning based an automated skin lesion segmentation and intelligent classification model,” *Journal of Ambient Intelligence and Humanized Computing*, vol. 12, no. 3, pp. 3245–55, 2021.

- [23] K. Shankar, E. Perumal, P. Tiwari, M. Shorfuzzaman and D. Gupta, "Deep learning and evolutionary intelligence with fusion-based feature extraction for detection of COVID-19 from chest X-ray images," *Multimedia Systems*, 2021. <https://doi.org/10.1007/s00530-021-00800-x>.
- [24] K. Shankar, Y. Zhang, Y. Liu, L. Wu and C. H. Chen, "Hyperparameter tuning deep learning for diabetic retinopathy fundus image classification," *IEEE Access*, vol. 8, pp. 118164–118173, 2020.
- [25] D. Potnuru, K. A. Mary and C. S. Babu, "Experimental implementation of flower pollination algorithm for speed controller of a BLDC motor," *Ain Shams Engineering Journal*, vol. 10, no. 2, pp. 287–295, 2019.